Available online at www.sciencedirect.com

ScienceDirect

journal homepage: www.elsevier.com/locate/issn/15375110

Research Paper

A novel hyperspectral line-scan imaging method for whole surfaces of round shaped agricultural products

Insuck Baek [a,b], *Byoung-Kwan Cho* [c], *Stephen A. Gadsden* [e], *Charles Eggleton* [a], *Mirae Oh* [b], *Changyeun Mo* [d,f], *Moon S. Kim* [b,*]

[a] Department of Mechanical Engineering, University of Maryland, Baltimore County, 1000 Hilltop Circle, Baltimore, MD, 21250, USA

[b] USDA-ARS Environmental Microbial and Food Safety Laboratory, Henry A. Wallace Beltsville Agricultural Research Center, Beltsville, MD 20705, USA

[c] Department of Biosystems Machinery Engineering, College of Agricultural and Life Science, Chungnam National University, 99 Daehak-ro, Yuseong-gu, Daejeon 34134, Republic of Korea

[d] National Institute of Agricultural Sciences, Rural Development Administration, 310 Nonsaengmyeong-ro, Wansan-gu, Jeonju-si, Jeollabuk-do 54875, Republic of Korea

[e] Intelligent Control and Estimation Laboratory, College of Engineering and Physical Sciences, University of Guelph, 50 Stone Road East, Guelph, ON, N1G 2W1, Canada

[f] Department of Biosystems Engineering, College of Agricultural and Life Sciences, Kangwon National University, 1 Gangwondaehakgil, Chuncheon-Si, Gangwon-Do, 24341, Republic of Korea

ARTICLE INFO

Article history:
Received 10 August 2018
Received in revised form
27 July 2019
Accepted 28 September 2019
Published online 26 October 2019

Keywords:
Apples
Whole surface inspection
Line-scan
3D reconstruction

The present study has developed a novel line-scan technique for hyperspectral imaging (HSI) of the whole surface of a round object. The developed system uniquely incorporates an external optical assembly of four mirrors to view a rotating round object from two opposite sides and project a combined two-view image onto the aperture of line-scan HSI camera. This allows imaging of the whole surface of the round object to detect defects located on any part of that surface. For obtaining the two side views that include the areas around the poles, the design of the optical path requires consideration of the distance from the inside mirrors to the outside mirrors, and the inclination angles of the outside mirrors. The optimum mirror distance of 171.6 mm and mirror angle of 13.24° was determined by sequential quadratic programming (SQP). The system was first calibrated using four wooden spheres of various sizes and was demonstrated for potential whole-surface imaging of round-shaped fruits by scanning 101 apples each marked with six simulated defects at known positions across the fruit surface. By using 3D reconstruction images, the system was able to accurately detect all six dots on 78% of the apples, but detected 5 dots (undercounted) and 7 dots (overcounted) on 4% and 18% of the apples, respectively. The image processing algorithm investigated in this study will be used to develop real-time

Abbreviations: HSI, hyperspectral imaging; FOV, Field of view; SQP, sequential quadratic programming; QP, quadratic programming.

* *Corresponding author*. Fax: +1 301 504 9466.
E-mail address: Moon.Kim@ars.usda.gov (M.S. Kim).

https://doi.org/10.1016/j.biosystemseng.2019.09.014
1537-5110/Published by Elsevier Ltd on behalf of IAgrE.

multispectral systems for whole-surface quality evaluation of rounded objects in the agro-food sector.

1. Introduction

Machine vision technology was introduced to the agro-food sector in the 1960s to overcome the constraints of laborious and time-consuming quality sorting performed by human inspectors, drawing significant attention from scientists and engineers during the following decades (Brosnan & Sun, 2004). Mimicking human eyes, machine vision systems rely on an RGB colour camera to capture images using three filters centred at red, green, and blue bands. The images can capture various external quality attributes such as size, shape, colour, and texture. Some defects can be detected with the application of image processing techniques (Zhang, Huang, Li, Zhao, Fan & Wu, 2014; Zhang, Wu, Qiu, & He, 2016). Fruits can be sorted and graded according to different quality level criteria. Even though machine vision technology has proven its effectiveness for some quality and safety measurements of agro-food products, its surface-colour-based discrimination capacity still has limitations. As the traditional machine vision technologies are limited to the measurement of physical and morphological properties of the target, detection of subtle defects like faecal contamination and internal damage require additional spectral information (Qin, Chao, Kim, Lu, & Burks, 2013; Zhang, Huang, Li, Zhao, Fan & Wu, 2014).

Regulations in many countries require fruit inspection to detect attributes beyond fundamental physical properties. For example, the U.S. Department of Agriculture (USDA) has standards for bruises, broken skin and cuts, internal browning, and mouldy stems, among other defects. Spectroscopic techniques have been proposed in many studies to cope with the issue of internal quality assessment (Wang, Peng, Xie, Bao, & He, 2015). While machine-vision-based systems use RGB cameras to detect light intensity primarily in three visible bands, more advanced spectral techniques divide the visible and near-infrared light into many spectral bands, ultimately enabling assessment of chemical and biological properties of agro-food products. However, the small point source commonly used in spectral assessment cannot provide spatial information.

Hyperspectral imaging (HSI), a combination of spectroscopy and imaging where the light spectrum is split into many narrow bands, was introduced to the agro-food sector for its capability to obtain both spatial and spectral features of a specimen (Kim, Chen, & Mehl, 2001). The spatial features of the hyperspectral image enable the characterisation of a complex heterogeneous sample, while the spectral features allow identification and quantification of surface and sub-surface multi-constituent characteristics.

For agricultural applications, the HSI technique has been increasingly used over the last decade as an effective tool for quality analysis of a wide range of agro-food products, accompanied by new advances in instrumentation as well as data analysis techniques to meet requirements for industrial use (Park et al., 2011). A range of studies have been conducted on fruit quality analysis in particular. ElMasry, Wang, ElSayed, and Ngadi (2007) tested the effectiveness of the HSI technique for non-destructive determination of moisture content, total soluble solids, and acidity in strawberries. Li, Wang, and Gu (2002) successfully detected common defects on oranges using HSI in the spectral region between 400 and 1000 nm. Kim, Burks, Ritenour, and Qin (2014) applied HSI for classifying citrus fruit samples into two classes, either with or without citrus black spot defect, with an accuracy of over 97%. Hyperspectral image analysis of apple fruits was used to identify the spectral features of apples in order to select optimal wavebands with which multispectral imaging systems could be designed for rapid detection of apple contamination (Mehl, Chao, Kim, & Chen, 2002), and to detect apple surface defects (Lee, Kang, Kim, & Noh, 2005).

Previous studies have demonstrated that HSI techniques are capable of accurately measuring quality and safety attributes of fruits, such as colour, texture, faecal contamination and bruises. In the process of developing multispectral imaging systems for possible real-time inspection line implementation, these investigations have focused on determining the optimal spectral imaging bands for specific applications. Due to hardware limitations, analysis of the entire spectrum in real time is impractical. In practical terms, reducing the total volume of the data to be processed enables the implementation of an efficient multispectral imaging system (Qin et al., 2013). Other key factors affecting the accuracy of a multispectral imaging system for online fruit inspection include light sources that illuminate the sample properly and, most importantly, the ability to scan the surface of the entire sample in order to detect all defects present.

Another critical factor in the design of an online inspection system is accessibility of the whole surface of the object being scanned. In contrast to the more uniform appearance of manufactured goods, any batch of agricultural products can have a range of sizes, shapes, and surface topography, despite all items being the same product. Thus, it is difficult to scan the whole surface, especially for relatively rounded objects. Despite these difficulties, whole-surface inspection is essential for sorting agricultural commodities to meet local and national requirements for geometric (e.g., diameter, volume) or surface texture (e.g., roughness) attributes. For example, any localised necrotic areas on fruit surfaces could lead to a negative perception of fruit quality on the part of consumers and affect their willingness to purchase and consume the fruit (Jaeger et al., 2016). Therefore, inspection of the entire surfaces of round fruits such as oranges and apples is a necessary step (Reese, Lefcourt, Kim, & Martin Lo, 2009).

However, HSI inspection methods effective for round shaped agricultural products such as apples, peaches and oranges have not been studied thoroughly. Some techniques previously investigated for assessing round objects require complex systems and/or multiple sensing units to cover the whole surfaces, thereby incurring additional costs and requiring more complex inspection procedures. A reliable method for presenting the entire surfaces of agro-food products to modern scanning devices should be an essential component of any effective sorting system. Even though several studies have investigated image-based inspection for entire fruit surfaces (Jiang, Zhu, Cheng, Luo, & Tao, 2009; Li et al., 2002; Molto, Blasco, & Benlloch, 1999), no commercial system is available for whole-surface inspection of round objects (Reese et al., 2009).

Previous studies have used a colour-based or multi-spectrum camera to obtain snapshots. The transitional system of apple grading using image analysis places the specimen on truncated-cone rollers and moves it perpendicularly to the field of view, which is the area of the inspection. This method can present two-thirds of the surface and is adequate to evaluate colour or size, but is insufficient for thorough defect inspection since surfaces near the rotation axis cannot be visualised. Throop, Aneshansley, Anger, and Peterson (2005) designed an inspection system using a kind of cup and small wheels. The apple is oriented so the stalk-calyx axis is vertical during the acquisition of the image. The apple is tilted by 45° and a surface image perpendicular to the optical axis of a camera is obtained. However, this system also does not consider the rotation area around the calyx and stalk poles. Molto et al. (1999) used robot arms to rotate an apple. This system was relatively accurate as robot arms manipulated the fruit for whole surface scanning, but led to low processing speed. The modelling of whole-surface imaging of apples using multiple mirrors below a wire-suspended fruit has also been investigated (Reese et al., 2009). However, because of the size variations of the fruits and a small shadow effect from the sample presentation method, producing a whole-surface image was not straightforward, and the method was inefficient for online applications for whole-surface imaging (Reese et al., 2009).

The objectives of this study were to: (1) investigate the capability of a single hyperspectral line-scan camera to be used in conjunction with mirrors to scan the whole surfaces of randomly oriented and rotating objects that model essentially round agro-products such as apples, peaches, and oranges, and (2) develop simple and efficient image processing algorithms capable of dealing with dynamic sample shapes and sizes in real time for implementation in an online inspection system.

2. Materials and methods

2.1. Hyperspectral image system design

The key sensing components of the laboratory-based hyperspectral line-scan imaging system are an imaging spectrograph (VNIR Concentric Imaging Spectrograph, Headwall Photonics, Fitchburg, MA, USA) and an electron-multiplying charge-coupled device (EMCCD) camera (Luca R DL-604M, 14-bit, Andor Technology, South Windsor, CT, USA) coupled to a C-mount objective lens (F1.4 17.6 mm compact lens, Schneider Optics, Hauppauge, NY, USA), as shown in Fig. 1. The EMCCD has 1002 × 1004 pixels. A 25-μm wide spectrograph aperture slit makes the instantaneous field of view into a thin line. A spheroidal or round object is placed on four truncated-cone rollers rotating at a steady speed (150 mm/s) that causes the object to rotate in place. Four truncated-cone rollers were controlled via a stepping motor (STP-MTRH-34127, 1.8°/step, Surestep, Taiwan). A 150-W quartz halogen light is split via fibre optic cable into two light sources mounted at 45° angles from the horizontal in order to uniformly illuminate both sides of the object. Operation of all the system components is coordinated through a computer program that was developed in Matlab software (version 7.04, Mathworks, Natick, MA, USA). This program manages not only the camera settings and image acquisition, but also settings for the initial speed of the stepping motors and angles of the outside mirrors. Stepping motors (42BYHH809, 0.9° step^{-1}, Wantai motor, China) cause micro-movements of the outside mirrors in order to change their relative angle with the light source. The camera of this system is capable of capturing images within the spectral region from 447 nm to 951 nm, but

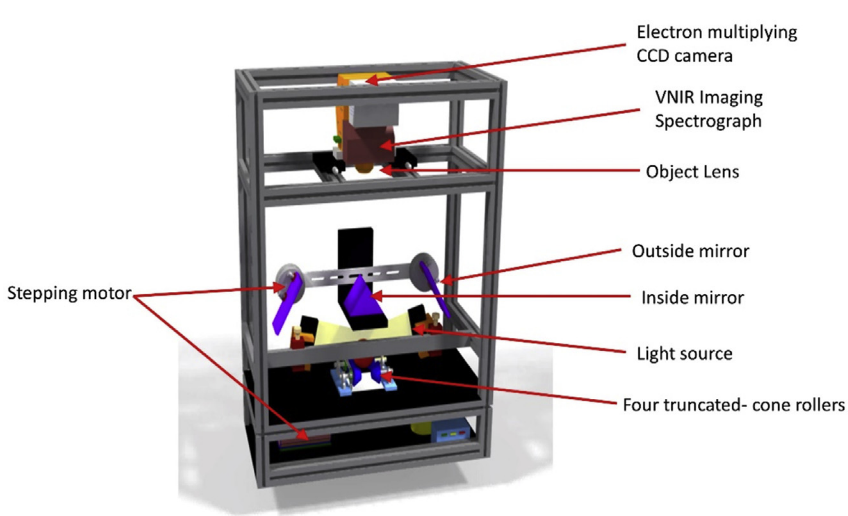

Fig. 1 – Schematic representation of HSI system for whole-surface line-scan imaging of a rounded object.

the program chooses only two bands which are within the user-determined region-of-interest wavelengths. The user can also choose prespecified wavelengths and spectral resolution (width of waveband).

For this study, two single-band images were taken simultaneously, at 572 and 723 nm since apple bruises were mainly distinguished at around 600 and 700 nm (Che et al., 2018). Non-contiguous bands were chosen for proof of concept, since two-waveband ratio algorithms have been used to identify spectral differences due to contaminants or defects of interest between the non-target and the target areas. Moreover, ratio algorithms have been effectively used to improve detection of defects and contaminants present on an object with various simple image processing methods, such as fuzzy logic, histogram thresholding, and spatial filtering (Keresztes, Goodarzi, & Saeys, 2016; Kim, Lefcourt, Chen, & Tao, 2005; Lefcourt & Kim, 2006). Five hundred line-images were acquired per object, resulting in hyperspectral image dimensions of 500 (lines) × 100 (spatial pixels) × 2 (spectral bands).

The HSI system for whole-surface round-object scanning has one inside mirror and two outside mirrors alongside to acquire two side views of a round object. As shown in Fig. 2, the inside mirror consists of two surface mirrors, with one abutting edge at a 90° angle. The image of a rotating round object is collected by the outside mirrors and then reflected onto the inside mirrors. The image gathered by the inside mirror is then reflected into the common aperture of the line-scan HSI camera.

A diffraction grating spectrograph in the hyperspectral camera disperses the line image from the inside mirror and then projects the line image onto the EMCCD. As mentioned above, even if the hyperspectral camera disperses a full-spectrum line image, the software focuses only on two specific wavebands of data to reduce the processing time.

2.2. *Optimisation of mirror position*

A single camera without any mirror assembly would not normally capture the areas of the round object near the poles (relative to the axis of rotation). In order to obtain the two side views that include the areas around the poles, the design of the optical path requires consideration of the distance from the inside mirror to the outside mirrors, and the inclination angles of the outside mirrors. A range of algorithms can be used for finding optimal distance and angle of the outside mirror. In this study, a sequential quadratic programming (SQP) procedure was employed to find the optimal position of the outside mirrors. SQP methods have evolved into a powerful and effective methods for diverse optimisation problems (Boggs & Tolle, 1995). SQP algorithms are used for nonlinearly constrained, gradient-based optimisation, supporting both equality and inequality constraints. The framework of SQP is described in the following steps. First step is set up and search direction from the solution to the quadratic programming (QP) sub-problem and then evaluate for convergence, if it is satisfied, stop. Second step is update new point along the search direction. Final step is update the Hessian matrix used in QP and repeat procedure. In this study, efforts were made to find optimal distances for the position of outside mirror. The feasible domain is defined as upper and lower bounds for each variable. Many practical optimisation problems are nonconvex, and applying traditional local optimisation methods may cause the search to stop when a local minimum is found. To find an optimal value, the initial value of the design variable was incremented by one within the feasible domain. Thus, we used initial distance value from 140 to 180 mm and initial angle value from 13 to 20°

2.3. *Development of model and sample preparation*

One of the objectives in this preliminary study is to demonstrate the efficiency of the whole-surface imaging method. For approaching whole-surface imaging, the first step is that the inside mirror is aligned with centre of the camera to divide the line-image into two equal-length line-images. After this first step, actual fields of view were made by adjusting outside mirror. Even though the inside mirror is aligned with centre of the camera, it is difficult to divide the line-image into two equal-length line-image. Before performing any experiments with round samples, spatial calibration of the system must

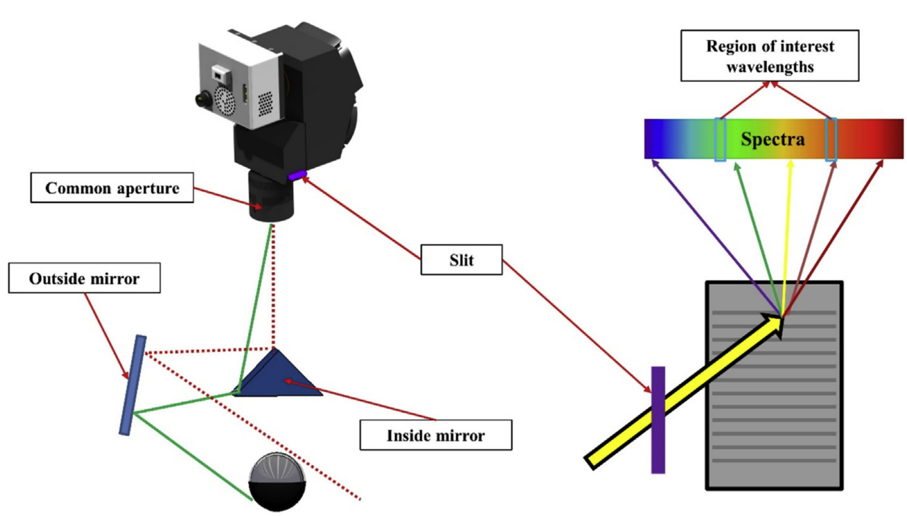

Fig. 2 – Diagram of the optical path (field of view) for capturing pole area of a round object.

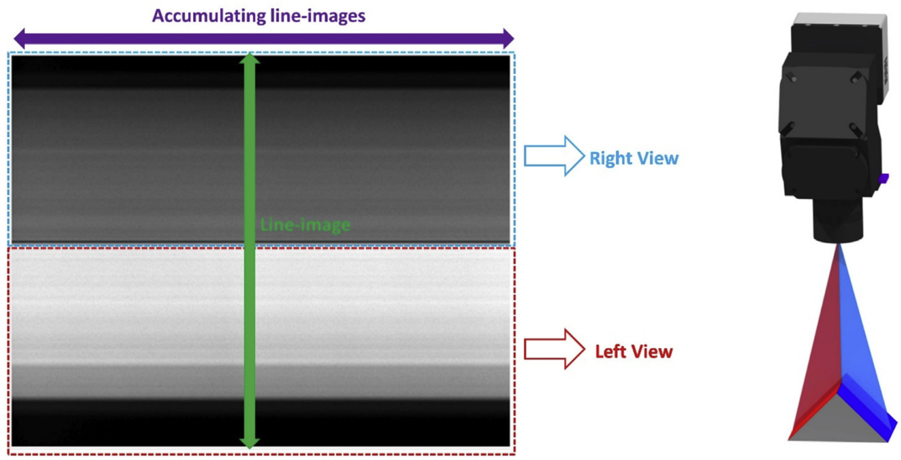

Fig. 3 – The spatial calibration image for division into the right and left fields of view (left) and the diagram of blue and red paper placed on the right and left sides of the inside mirror (right).

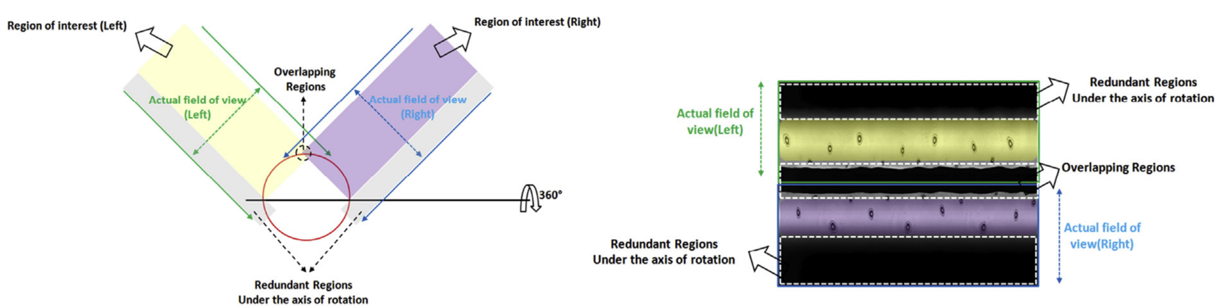

Fig. 4 – Schematic (left) shows the principle of the two-view-angle line-scanning arrangement for capturing the whole surface of a rotating round object. Unsegmented raw image (right) shows the FOVs and areas corresponding to the schematic (left) for whole-surface imaging. The line-scan FOV of the imaging system is aligning to the axis of rotating apple.

precisely divide the image into the right and left line-images since image processing methods are applied to each line-image. An image was captured with blue and red paper placed on the right and left faces of the inside mirror, respectively. Figure 3 shows the inside mirror covered with blue and red and the corresponding right and left views in the resulting image. Raw image data was separated into the right image and left image from the captured line-images based on this spatial calibration step.

Figure 4 gives a detailed account of the actual field of view and an unsegmented two-view-angle image. Once the images are collected by the line-scan camera, only the areas acquired above the axis of rotation (along the upper semicircle of the sample in Fig. 4) are needed to inspect the whole surface. The acquired image areas from below the axis of rotation, and from the overlapping region at the top, contain unnecessary duplicated information that, if retained, can lead to increased image processing time and errors. Thus, the overlapping and redundant regions must be removed to efficiently acquire a 360° image of the sample. To develop the image processing algorithm, four wooden spheres with diameters of 76.2, 88.9, 101.6 and 114.3 mm were scanned in order to optimise the position of outside mirrors. Six dots were placed on the surface of each wood sphere, and were used to verify that the developed system can cover or inspect the whole surface. The

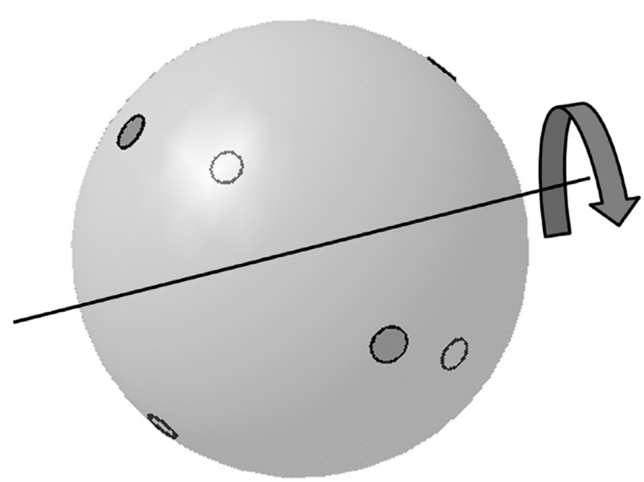

Fig. 5 – Schematic of wood sphere showing the positions of dots.

Table 1 – Summary of descriptive statistics for the apple samples used to validate the model.

Cultivar	Quantity	Circumference (Major/Minor)			
		Average (mm)	Max (mm)	Min (mm)	Standard Deviation
Honeycrisp	36	30.1/29.7	33/32.5	27.5/26.7	1.55/1.91
Gala	26	23.4/23.8	25.2/26.3	21.0/21.3	1.28/1.49
Fuji	19	24.9/24.8	28.8/28.1	20.4/19.5	2.93/2.89
McIntosh	10	25.0/24.0	26.3/24.8	23.0/22.5	1.07/0.81
Red Delicious	10	25.0/24.9	26.1/26.0	24.0/23.5	0.59/0.73
Total	101	26.4/26.2	33.0/32.5	20.4/19.5	3.34/3.22

six dots were placed manually at the north pole, south pole, 0° and 90° west longitude, and 0° and 90° east longitude, as shown in Fig. 5.

To test the model for a round agro-product, six dots were painted on the surface of an apple at the same locations as indicated for the wood sphere. The image processing method developed using the wood spheres was then applied to process the collected apple images. A total of 101 apples were each randomly oriented and rotated on the rollers for imaging, and a whole-surface image for each apple sample was produced with the mirror system. The descriptive statistics of the apple samples used are given in Table 1. Five different cultivars of apples with different sizes and shapes were selected to show the effectiveness of developed system for handling the physical variation in the samples.

3. Results and discussion

3.1. *Outside mirror configuration*

To efficiently reconstruct 3D images, it was necessary to minimise the redundant and overlapping regions by controlling the distance and angle of the outside mirror, since the FOV depends on the position of outside mirror as shown in Fig. 2. An object function by deriving Eq. (1) and Eq. (2) of a straight line using the original camera the FOV and reflection laws was constructed. The unknowns x_2 and y_2, related to Eq. (2), can be calculated by Eq. (3) and Eq. (4),

$$y = \tan(2\alpha)x + H_1 - \tan(2\alpha)d \tag{1}$$

$$y = \tan(12.8 + 2\alpha)x + y_2 - tan(12.8 + 2\alpha)x_2 \tag{2}$$

$$\begin{aligned}&[\tan(-12.8)x_2 + H_2 - \tan(-12.8)53.05]\\&-[tan(\alpha-90)x_2 + H_1 - \tan(\alpha-90)d] = 0\end{aligned} \tag{3}$$

$$y_2 = \tan(-12.8)x_2 + H_2 - \tan(-12.8)53.05 \tag{4}$$

where α is the angle of the mirror as shown in Fig. 6, d is the distance between the inside mirror and the outside mirrors, H_1 is the height from centre of sample target to top of the inside mirror, and H_2 is the height from centre of target to the bottom of the inside mirror.

The object function (Eq. 5) and two constraints (Eqs. 6 and 7) were made by the following steps. First of all, the best way to make the 3D reconstruction image is to obtain the FOV passing through the two red dots as marked in Fig. 6. Simply, Eq. (1) intersects the first red dot at the top and Eq. (2) intersects the red dot at the bottom. However, for this ideal optical path, it is hard to get the FOV of the camera to pass through those two red dots. Thus, both equation lines must include both red dots, accomplished by controlling the distance and angle of the mirror. If the FOV does not include both red dots, then essential image information for the capturing the whole surface of the sample will be missed. For minimising the object function, we subtracted Eq. (1) from Eq. (2) at x equal to 0. For example, more space is gained when those two lines are far away from each other, which ensures that both red dots are included, but more unnecessary surface area related to the whole surface is also gained. So, the distance between the two lines should be minimised as much possible while including both red dots. To place the two red dots between Eqs. (1) and (2), two constraints were created. The first constraint is that the y-intercept of Eq. (1) must be larger than the object radius, and the second constraint is that the x-intercept of Eq. (2) must be larger than the object radius.

$$\begin{aligned}\textit{Object function}: \min f(\alpha, d) = (H_1 - \tan(2\alpha)d)\\ - (y_2 - \tan(12.8 + 2\alpha)x_2)\end{aligned} \tag{5}$$

$$g_1 = r - H_1 + \tan(2\alpha)d \le 0 \tag{6}$$

$$\begin{aligned}&g_2 = r + \frac{y_2 - \tan(12.8 + 2\alpha)x_2}{\tan(12.8 + 2\alpha)} \le 0\\&\alpha, d > 0\end{aligned} \tag{7}$$

where r is the radius of the target.

Using the optimisation process described above, it was determined that an outside mirror distance of 171.6 mm and angle of 13.24° minimise the object function while covering all six dots on the surface of each of the four wooden spheres.

3.2. *Development of image processing algorithm*

Figure 7 illustrates the image processing used to scan the whole surface for inspection. The first step in processing the original image is to remove the border background area under the axis of rotation, as shown in the top half of Fig. 7. Afterward, the second step is to apply a centring process to the image, as shown in the top half of Fig. 7. The centring process moves the white apple area to the bottom of the rectangle in the right part image and to the top of the rectangle in the left part image. In order to consistently process the overlapping

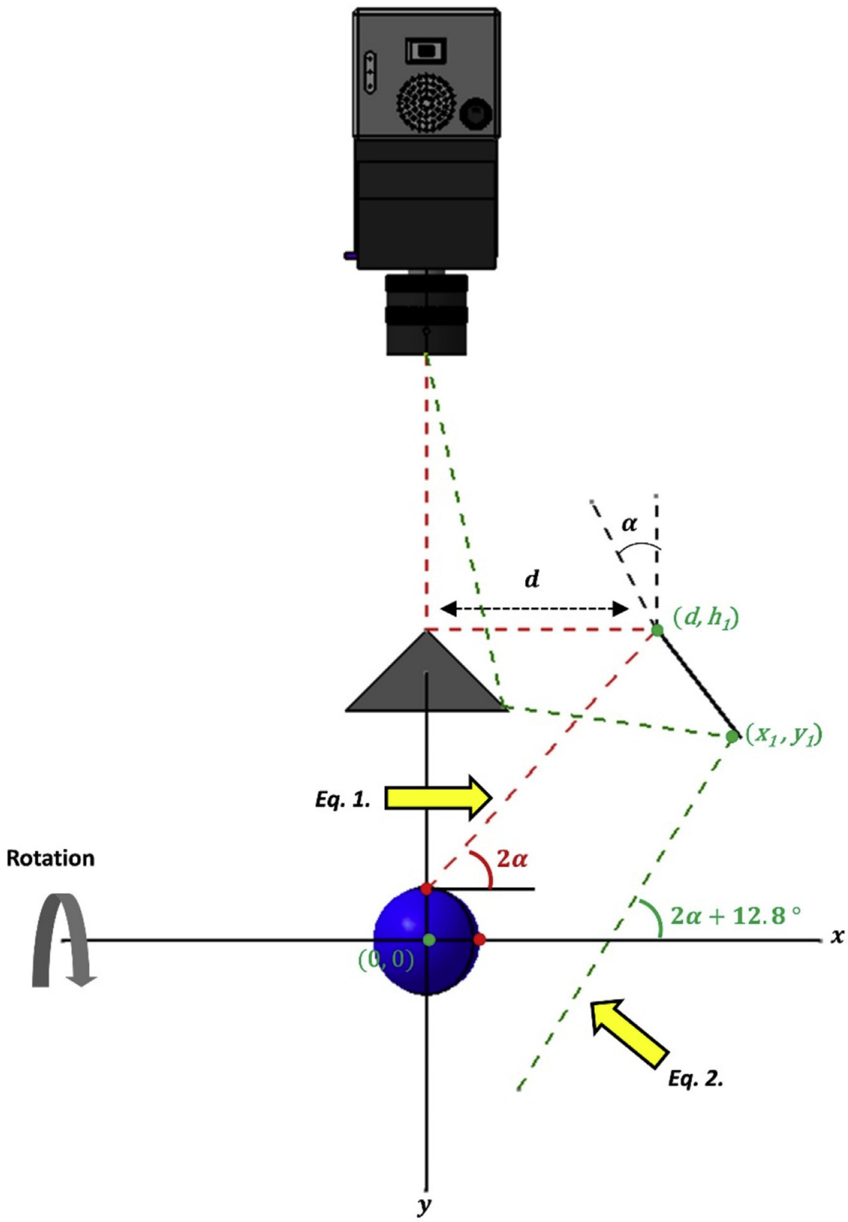

Fig. 6 – Schematic shows the optical path as dependent on position of mirror, object function and two constraints.

areas regardless of object size, the left and right image areas are offset either up or down to the centreline, and then the overlapping area is removed. Even though the outside mirrors are controlled by a micro-stepping motor, a small difference in the angle of the left- and right-side mirrors requires the columns to be re-aligned. Following the previous image processing of the two side-view images, the circumference or the number of the line-scan images required to cover the whole surface in rotation is estimated by calculating the number of vertical black (background) pixels between right and left image, since the vertical pixel distance is constant (and depends on the target size). A linear regression equation relating vertical pixel number to the number of line scans needed to image 360 degrees of the object was developed using the four wooden spheres at the optimal angle and distance. The resulting line is given below and shown in Fig. 8. The following regression equation can be used to automatically estimate the number of line scans required since the diameter of the samples to be inspected varies,

$$y = -0.2114x + 175.8 \tag{8}$$

where y is number of line-scans for 360° and x is number of vertical image pixels.

The whole-surface image acquisition method was calibrated using round objects of known diameters. Last but not least, the rectangular line-scan image of the round object was projected onto a spherical surface for 3D reconstruction.

3.3. *Proof of algorithm*

Next, effective use of the single HSI camera with mirror assembly to scan the entire surface of a round object was

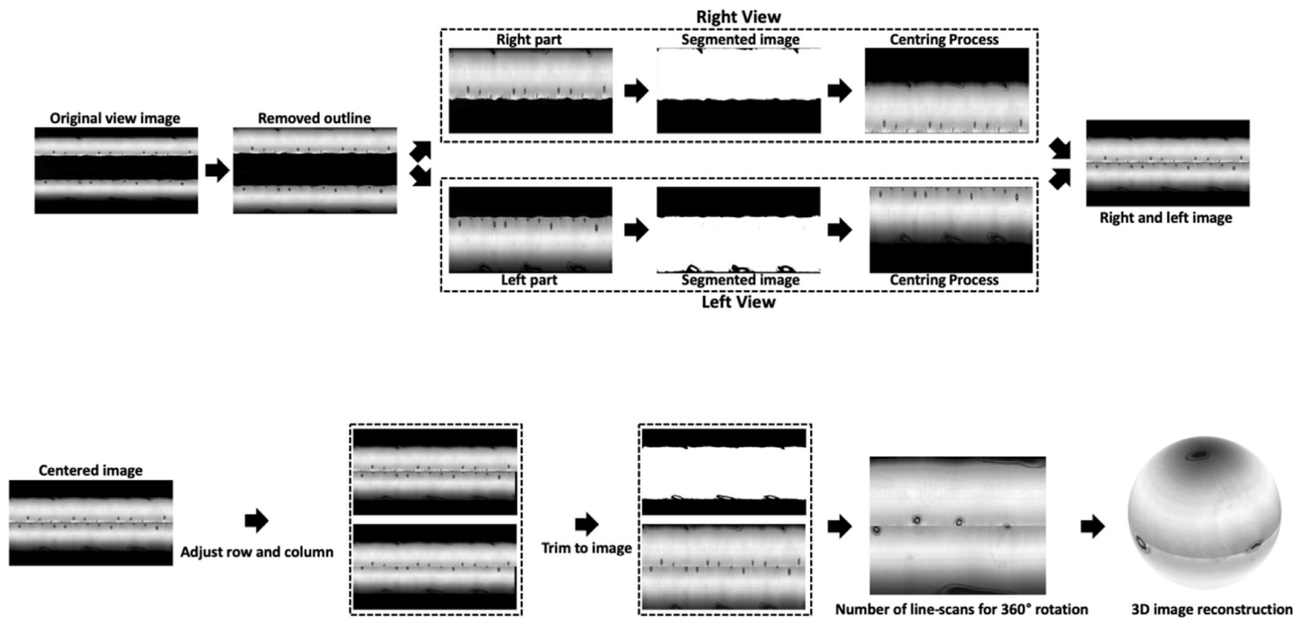

Fig. 7 – Image segmentation procedure used to scan the whole surface of a round sample for inspection.

demonstrated using apple fruits each marked with six dots as simulated defects. A 3D-reconstructed image of apples was produced by using the optimal angle 13.24° and distance of 171.6 mm and first regression Eq. (8). Table 2 details the results for the numbers of dots observed in the processed images of the apples. The hyperspectral line-scan image with mirrors was able to detect six individual dots per apple image for 78% of the 101 apples. Five dots were observed in 4% of the apple images, and seven dots were observed in 18% of the apple images. The apples for which six dots were observed had an average difference of 0.71 mm between the lengths of their major and minor circumferences. On the other hand, the apples for which seven or five dots were observed had average differences of 0.87 and 0.76 mm, respectively, between the lengths of their major and minor circumferences. These results indicate that the whole-surface imaging accuracy increases when the object is more spherical. From the point of view of inspection for contaminants and defects for food safety in commercial agriculture, the sorting system can deal with over-counting of defects. However, detection of only five dots means that the defects were undercounted, implying that the whole surface of the fruit was not inspected. This may have resulted from bouncing or wobbling of the apple during rotation on the four truncated-cone rollers.

Resultant images of an apple were acquired at multiple azimuthal positions and elevation viewpoints, as illustrated in Fig. 9. The reconstructed images projected onto spherical surfaces are shown for six pairs of azimuthal angle and viewpoint elevation in Fig. 9, and the dot were counted by manually. For counting the dots on reconstructed images, if a part of the dot appeared, it was recognised as a dot since it is indicated covering whole surface (about >95%). The dashed red circles in Fig. 9 indicate more severely distorted dots. The distortion might be due to the fact that axis of rotation is not fixed and the principle of optical projection called the morphological curvature effect. Seven dots were observed in 18% of the test samples since the shape of an apple is not perfectly spherical, which leads to over estimation of the number of line-scans for one rotation by the first regression equation. The blue-dotted box area indicates the over-estimated area in Fig. 10. An enhancement in regression

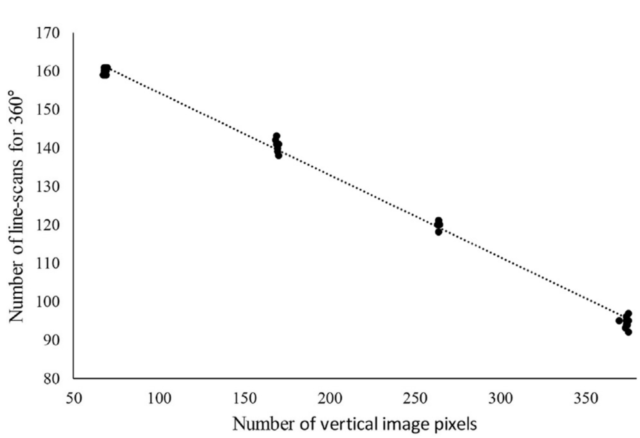

Fig. 8 – Relationship between number of vertical image pixels and number of line-scans for 360° imaging.

Table 2 – Results for observed number of dots on imaged apple surfaces.

Cultivar (quantity)	Observed number of dots in apple image (accuracy)		
	5	6	7
Honeycrisp (36)	1 (2.78%)	28 (77.78%)	7 (19.44%)
Gala (26)	1 (3.85%)	21 (80.76%)	4 (15.38%)
Fuji (19)	2 (10.52%)	14 (73.68%)	3 (15.79%)
Mcintosh (10)	0 (0%)	8 (80%)	2 (20%)
Red delicious (10)	0 (0%)	8 (80%)	2 (20%)
Total (101)	4 (3.96%)	79 (78.21%)	18 (17.82%)

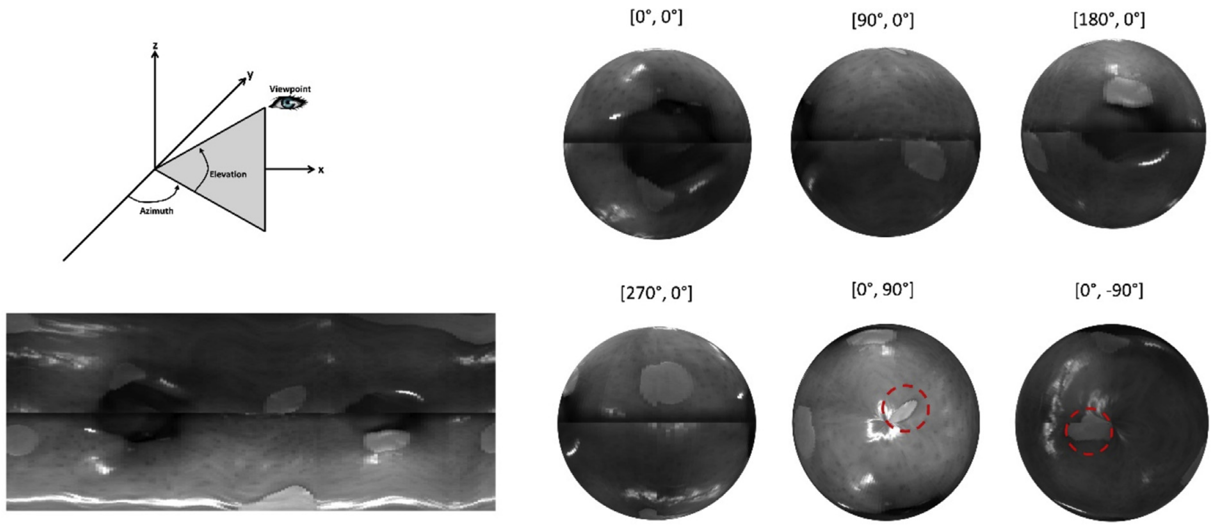

Fig. 9 – Rectangular whole-surface representation of apple in line-scan image, and illustration of spherical image transformation highlighting each of the six detected dots on the apple.

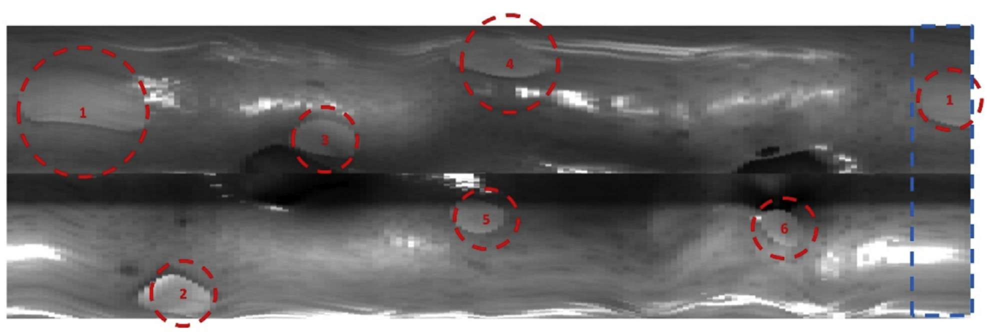

Fig. 10 – Whole-surface representation of apple in line-scan image with overestimated region showing seventh dot.

model for estimating number of line-scans to determine one complete rotation of an apple is needed by incorporating various size apples in the model development.

In practise, an automated apple grading and inspection system based on machine vision must identify the stem-ends and calyxes in apple images, since stem-ends and calyxes could be potentially misclassified as a defect. The major advantage of the current whole-surface imaging approach is that an apple exhibiting only two spots (i.e., stem and calyx) could be automatically classified as a sound apple. This would mitigate some complexities in image processing, to specifically identify stem-ends and calyxes on apple images using multispectral images as demonstrated by earlier studies (Jiang et al., 2009; Xing, Jancsók, & Baerdemaeker, 2007).

4. Conclusion

Improvements in imaging hardware have resulted in simple and reliable technology that can be used to automate the inspection of agro-products. The capabilities of the older RGB systems make them excellent replacements for manual labour when considering the sorting of agro-products based on size and shape. However, standards worldwide require inspection for contaminants and other defects that can be detected by spectral imaging systems. As a result, many studies have focused on optimising spectral wavebands with reduced data size in order to scan agro-products and process the images in real-time. A challenge faced by spectral imaging systems is optical access to the whole surface of the agro-product. In this study, two-view-angle optics are placed between a single line-scan imaging object lens and a rotating round object to simultaneously capture images of both hemispheres. This hyperspectral line-imaging system produces an image representation of the entire surface of the round object as a rectangular-shaped projection, unlike conventional imaging of round objects that produce hemispherical views as circular projections. After the resulting images are processed to remove redundant data, 3D images can be reconstructed through projection onto a spherical surface. Calibration tests showed that the system could detect six simulated defects dispersed evenly over the surface of an apple, without missing or repeating a defect, for 78% of the apple fruits tested in this study. Even though this system cannot reconstruct the original shape of the target, the mirror enables the system to inspect the polar areas that a conventional single-camera system cannot cover. That is an important factor for inspectors tasked with ensuring food safety and seeking cost-effective inspection systems. This novel whole-surface line-scan HSI system can be implemented in combination with current automated screening and sorting systems used in agro-industry. Further study is required to consider agro-products of varying sizes and shapes for real-time inspection.

Funding

This work was supported by the USDA Agricultural Research Service, Food Safety National Program [Project No. 8042-42000-020-00D]; and the National Institute of Agricultural Sciences, Rural Development Administration, Republic of Korea [Research Program for Agricultural Science & Technology Development, Project No. PJ012216].

Declaration of interest

The authors declare no conflicts of interest.

Acknowledgements

Authors would like to thank Ms. Diane Chan of the Environmental Microbial and Food Safety Laboratory, ARS, USDA, for proofreading the manuscript.

REFERENCES

Boggs, P. T., & Tolle, J. W. (1995). Sequential quadratic programming. *Acta Numerica, 4*, 1. https://doi.org/10.1017/S0962492900002518.

Brosnan, T., & Sun, D.-W. (2004). Improving quality inspection of food products by computer vision––a review. *Journal of Food Engineering, 61*(1), 3–16. https://doi.org/10.1016/S0260-8774(03)00183-3.

Che, W., Sun, L., Zhang, Q., Tan, W., Ye, D., Zhang, D., et al. (2018). Pixel based bruise region extraction of apple using Vis-NIR hyperspectral imaging. *Computers and Electronics in Agriculture, 146*, 12–21. https://doi.org/10.1016/j.compag.2018.01.013.

ElMasry, G., Wang, N., ElSayed, A., & Ngadi, M. (2007). Hyperspectral imaging for nondestructive determination of some quality attributes for strawberry. *Journal of Food Engineering, 81*(1), 98–107. https://doi.org/10.1016/j.jfoodeng.2006.10.016.

Jaeger, S. R., Antúnez, L., Ares, G., Johnston, J. W., Hall, M., & Harker, F. R. (2016). Consumers' visual attention to fruit defects and disorders: A case study with apple images. *Postharvest Biology and Technology, 116*, 36–44. https://doi.org/10.1016/j.postharvbio.2015.12.015.

Jiang, L., Zhu, B., Cheng, X., Luo, Y., & Tao, Y. (2009). 3D surface reconstruction and analysis in automated apple stem-end/calyx identification. *Transactions of the ASABE, 52*(5), 1775–1784. https://doi.org/10.13031/2013.29118.

Keresztes, J. C., Goodarzi, M., & Saeys, W. (2016). Real-time pixel based early apple bruise detection using short wave infrared hyperspectral imaging in combination with calibration and glare correction techniques. *Food Control, 66*, 215–226. https://doi.org/10.1016/j.foodcont.2016.02.007.

Kim, D., Burks, T. F., Ritenour, M. A., & Qin, J. (2014). Citrus black spot detection using hyperspectral imaging Daegwan. *International Journal of Agricultural and Biological Engineering, 7*(6), 20–27. https://doi.org/10.3965/j.ijabe.20140706.004.

Kim, M. S., Chen, Y. R., & Mehl, P. M. (2001). Hyperspectral Reflectance and Fluorescence imaging system for Food quality and safety. *Transactions of the ASAE, 44*(3), 721–729. https://doi.org/10.13031/2013.6099.

Kim, M. S., Lefcourt, A. M., Chen, Y.-R., & Tao, Y. (2005). Automated detection of fecal contamination of apples based on multispectral fluorescence image fusion. *Journal of Food Engineering, 71*(1), 85–91. https://doi.org/10.1016/j.jfoodeng.2004.10.022.

Lee, K.-J., Kang, S., Kim, M. S., & Noh, S.-H. (2005). Hyperspectral imaging for detecting defect on apples. In *2005 Tampa, FL July 17–20, 2005*. St. Joseph, MI: American Society of Agricultural and Biological Engineers.

Lefcout, A. M., & Kim, M. S. (2006). Technique for normalizing intensity histograms of images when the approximate size of the target is known: Detection of feces on apples using fluorescence imaging. *Computers and Electronics in Agriculture, 50*(2), 135–147. https://doi.org/10.1016/j.compag.2005.10.001.

Li, Q., Wang, M., & Gu, W. (2002). Computer vision based system for apple surface defect detection. *Computers and Electronics in Agriculture, 36*(2–3), 215–223. https://doi.org/10.1016/S0168-1699(02)00093-5.

Mehl, P. M., Chao, K., Kim, M., & Chen, Y. R. (2002). Detection of defects on selected apple cultivars using hyperspectral and multispectral image analysis. *Applied Engineering in Agriculture, 18*(2). https://doi.org/10.13031/2013.7790.

Molto, E., Blasco, J., & Benlloch, J. V. (1999). Computer vision for automatic inspection of agricultural produce. In G. E. Meyer, & J. A. DeShazer (Eds.), *SPIE the international society for optical engineering* (pp. 91–100).

Park, B., Yoon, S.-C., Windham, W. R., Lawrence, K. C., Kim, M. S., & Chao, K. (2011). Line-scan hyperspectral imaging for real-time in-line poultry fecal detection. *Sensing and Instrumentation for Food Quality and Safety, 5*(1), 25–32. https://doi.org/10.1007/s11694-011-9107-7.

Qin, J., Chao, K., Kim, M. S., Lu, R., & Burks, T. F. (2013). Hyperspectral and multispectral imaging for evaluating food safety and quality. *Journal of Food Engineering, 118*(2), 157–171. https://doi.org/10.1016/j.jfoodeng.2013.04.001.

Reese, D., Lefcourt, A. M., Kim, M. S., & Martin Lo, Y. (2009). Using parabolic mirrors for complete imaging of apple surfaces. *Bioresource Technology, 100*(19), 4499–4506. https://doi.org/10.1016/j.biortech.2008.11.059.

Throop, J. A., Aneshansley, D. J., Anger, W. C., & Peterson, D. L. (2005). Quality evaluation of apples based on surface defects: Development of an automated inspection system. *Postharvest Biology and Technology, 36*(3), 281–290. https://doi.org/10.1016/j.postharvbio.2005.01.004.

Wang, H., Peng, J., Xie, C., Bao, Y., & He, Y. (2015). Fruit quality evaluation using spectroscopy technology: A review. *Sensors, 15*(5), 11889–11927. https://doi.org/10.3390/s150511889.

Xing, J., Jancsók, P., & De Baerdemaeker, J. (2007). Stem-end/Calyx identification on apples using contour analysis in multispectral images. *Biosystems Engineering, 96*(2), 231–237. https://doi.org/10.1016/j.biosystemseng.2006.10.018.

Zhang, B., Huang, W., Li, J., Zhao, C., Fan, S., Wu, J., et al. (2014). Principles, developments and applications of computer vision for external quality inspection of fruits and vegetables: A review. *Food Research International, 62*, 326–343. https://doi.org/10.1016/j.foodres.2014.03.012.

Zhang, W., Wu, X., Qiu, Z., & He, Y. (2016). A novel method for measuring the volume and surface area of egg. *Journal of Food Engineering, 170*, 160–169. https://doi.org/10.1016/j.jfoodeng.2015.08.025.